CHAPTER 4

ROBUST SPEED CONTROL OF THE SMPMSM DRIVE

4.1 Introduction

As described in the previous chapter, the proposed control strategy can achieve both fast dynamics and minimum copper loss operation. A PI speed controller is used in the outer loop to compensate the characteristics so that the drive can keep up a high performance operation in spite of the load torque disturbance. However, it is well known that the performance of the PI speed controller is sensitive to the variation of plant parameters and external disturbances. Some control strategies have been proposed to overcome the above problem. In [54], a full-order load torque observer is proposed to estimate the inaccessible load torque and then the estimated load torque is fed to the controller to upgrade the robustness of the drive system. Furthermore, a reduced-order observer instead of the full-order observer can be made due to the known measured rotor speed. On the other hand, the sliding mode control (SMC) strategy was also proposed to improve the robustness of the drive system [48-54]. The SMC possesses some good control features, such as disturbance rejection, parameter insensitive, fast dynamics and easy implementation. To reject the disturbance, the control signal of the SMC may be switched between its minimum and maximum values. Consequently, the resulting high frequency chattering may increase the power loss and excite the un-modeled high frequency dynamics which may deteriorate the system stability. In addition, some control efforts must be paid to deal with the disturbance rejection. When chattering problem is serious, it is difficult to utilize the maximum available torque of the drive. Hence, some methods were proposed to reduce the chattering problem [48-54]. Among them, an adaptive uncertainty observer was proposed to relax the bound of the lumped uncertainty [47]. Due to the limitation

of maximum available torque in the field weakening region, there are very few literatures dealing with the SMC operated in the field weakening region for the SMPMSM drive.

In this chapter, first, a sliding-mode speed controller with an adaptive strategy for estimating the lumped uncertainty is proposed to relax the requirement for the upper bounds of the lumped uncertainty. By combining the sliding-mode speed controller and the drive control strategy proposed in chapter 3, the conventional PI speed controller is replaced by the sliding-mode speed controller to further improve the rejection capability to disturbance. Finally, some simulation and experimental results are given to verify the validity of the proposed adaptive sliding mode speed controller

.

4.2 Robust Speed Control via an adaptive SMC Approach

Since the bandwidth of the current loop is greatly wider than that of the speed loop, the current-regulated PWM inverter can be considered as an ideal current amplifier to the design the speed controller. If the current-regulated PWM inverter is considered as an ideal current amplifier, namely $i_{ds}^{*} = i_{ds}$ and $i_{qs}^{*} = i_{qs}$, the SMPMSM drive system with such ideal inverter can be reasonably represented by the following equation

$$J\frac{d\omega_r}{dt} + B\omega_r + T_L = K_t i_{qs}^{*} \tag{4.1}$$

where J, B and T_L denote the inertia coefficient, viscous damping coefficient and external load torque respectively, and $K_t = \frac{3}{2}\frac{p}{2}\lambda_f$ denotes the torque constant.

If uncertainties are considered, equation (4.1) can be modified as follows:

$$(J_o + \Delta J)\frac{d\omega_r}{dt} + (B_o + \Delta B)\omega_r + T_L = K_t i_{qs}^{*} \tag{4.2}$$

where J_o and B_o denote the nominal values and $\Delta J = J - J_o$ and $\Delta B = B - B_o$ denote the variations of J and B, respectively.

Thus, from equation (4.2), one can obtain

$$\frac{d\omega_r}{dt} \equiv -a_o\omega_r - b_o i_{qs}^{*} - d_o f \tag{4.3}$$

where $a_o = \frac{B_o}{J_o}$, $b_o = -\frac{K_t}{J_o}$, $d_o = \frac{1}{J_o}$ and f denotes the lumped uncertainty defined as :

$$f = T_L + \Delta J \frac{d\omega_r}{dt} + \Delta B\omega_r \tag{4.4}$$

If the speed error is defined as $e = \omega_r^{*} - \omega_r$ under the assumption that the speed command reference ω_r^{*} is constant, the resultant error dynamic equation is derived as

$$\frac{de}{dt} = a_o\omega_r + b_o i_{qs}^{*} + d_o f \tag{4.5}$$

The above lumped uncertainty, namely f, cab be estimated and compensated through feedforward compensation.

Due to the disadvantages of PI speed controller, a sliding-mode speed controller with adaptive strategy is proposed to replace the conventional PI speed controller. Moreover, the adaptation of the lumped uncertainty can relax the need of the upper bound of the lumped uncertainty in the reaching-mode control. Designs of the speed controller and adaptation law for the lumped uncertainty are described as follows:

A. Sliding surface design of the sliding-mode speed controller

A sliding function is chosen as follows:

$$s = e = \omega_r^{*} - \omega_r \tag{4.6}$$

Usually, an integral operation is used to achieve the objective of zero steady-state error in the existing literatures. Although an integral operation is not included in the proposed sliding function, the objective of zero steady-state error is still achieved through the utilization of the estimated lumped uncertainty.

B. Adaptation law for the lumped uncertainty of the sliding-mode speed controller

Usually, the sliding-mode controller requires the upper bound of the lumped uncertainty to ensure that the reaching mode condition, $s\,\dot{s} < 0$, is satisfied. The reaching mode condition can guarantee that the system dynamics will be strapped on the sliding surface when the system dynamics is outside the sliding surface. Normally, the chattering phenomenon will become serious if the upper bound is over specified. On the contrary, if the upper bound is underspecified then the stability of the drive system can not be guaranteed under the effect of lumped uncertainty. Unfortunately, the exact value of the upper bound of the lumped uncertainty is usually difficult to obtain and specify in advance for most of industrial applications. Therefore, the upper bound is generally estimated to fulfill the requirement of the reaching mode condition. To achieve a compromise between the reduction of chattering and the system stability, an adaptive strategy for the lumped uncertainty is proposed in this chapter. Meanwhile, the exponential decay characteristic of the speed error is still required. Therefore, the q-axis current command i_{qs}^{*} can be decomposed into three components as follows to achieve both requirements of the reaching mode condition and the reduction of the chattering phenomenon, simultaneously.

$$i_{qs}^{*} = i_{qe}^{*} + i_{qr}^{*} + i_{qf}^{*} \tag{4.7}$$

where i_{qe}^{*} denotes the equivalent control effort, i_{qr}^{*} denotes the

reaching-mode control effort to ensure that the reaching mode condition will be satisfied, and i_{qf}^{*} is the control effort to reject the estimated lumped uncertainty $\hat{f}$.

To guarantee the stability of the proposed speed controller, i_{qr}^{*} and i_{qf}^{*} must be designed so that the reaching mode condition and the exponential decay characteristics for both s and the estimated error be guaranteed simultaneously.

First, consider the estimated error of the lumped uncertainty as defined previously:

$$\tilde{f}(t) \equiv f - \hat{f}(t) \tag{4.8}$$

Then, a positive definite Lyapunov function candidate, $V(t)$, is chosen as follows:

$$V(t) = \frac{1}{2}[s^2 + \frac{1}{\rho}\tilde{f}^2] \tag{4.9}$$

where $\rho > 0$ denotes the adaptation gain.

The derivative of $V(t)$ can be obtained from (4.5)-(4.9) as follows:

$$\dot{V}(t) = s\,[(b_0\, i_{qe}^{*} + a_0\, \omega_r) + (b_0\, i_{qf}^{*} + d_0\, \hat{f}) + b_0\, i_{qr}^{*}] + \tilde{f}(s\, d_0 - \frac{1}{\rho}\, \dot{\hat{f}}) \tag{4.10}$$

One can choose i_{qr}^{*}, i_{qf}^{*}, i_{qe}^{*} and the adaptation law of $\hat{f}$ so as to make $\dot{V}(t)$ being semi-negative definite as follows:

$$i_{qe}^{*} = -\frac{a_0}{b_0}\,\omega_r \tag{4.11}$$

$$i_{qf}^{*} = -\frac{d_0}{b_0}\,\hat{f} \tag{4.12}$$

$$i_{qr}^{*} = k\ |s|\ sign(s) \tag{4.13}$$

$$\dot{\hat{f}} = \rho\ s\ d_0 \tag{4.14}$$

where k is a designed constant and it must be greater than zero to guarantee the reaching mode condition. From equations (4.11)-(4.14), a variable gain which is proportional to $|s|$, is utilized to determine the necessary reaching-mode control effort so as to reduce the excessive chattering. In addition, $\hat{f}$ is considered as lumped uncertainty and can be rejected feedforward. Due to the integral adaptation of equation (4.14), the proposed controller can achieve the objective of zero steady-state error even that an integral operation is not included in the sliding function $s(t)$.

Due to the above design, $\dot{V}(t)$ is semi-negative definite. Since $V(s(0), \tilde{f}(0))$ and $\dot{V}(s)$ are bounded and $\dot{V}(t)$ is bounded and semi-negative definite, according to Barbalat lemma [61], the following result can be obtained:

$$s \to 0 \qquad \text{as t} \to \infty$$

As discussed above, the lumped uncertainty can be estimated and rejected by the proposed adaptive sliding-mode speed controller. Thus, excessive additional control energy in the field weakening region can be eliminated and the chattering phenomenon can be reduced effectively. The proposed robust speed control strategy can be implemented with the same structure as shown in Fig 3.1 except that the conventional PI speed controller is replaced by the proposed adaptive sliding-mode speed controller which is shown in Fig 4.1. The corresponding simulation results of the proposed control strategy are provided in the next section.

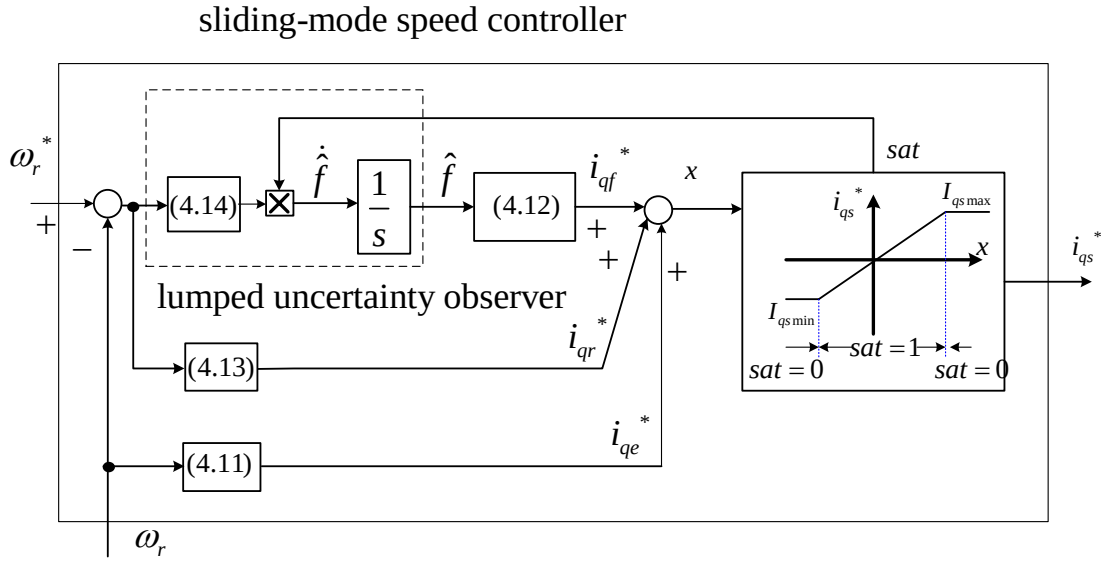

Fig 4.1. Configuration of the sliding-mode speed controller with adaptive lumped uncertainty observer.

4.3 Simulation results

In order to verify the feasibility of the proposed adaptive sliding-mode speed controller, computer simulations are performed in this section. For consistency, the nominal parameters of the simulated SMPMSM are kept the same as that in the section 3.3 and Table 2.1. These nominal parameters are utilized for the following simulation. Moreover, the dc link voltage is assumed to be 100 V. The following simulations are based on the same structure shown in Fig. 3.1, except that the conventional PI speed controller is replaced by the adaptive sliding-mode speed controller. Also, the adopted speed control configuration is shown in Fig 4.1. In the following simulations, the values of ρ and k are choose as 0.075 and 1.126, respectively.

First, to demonstrate the high accelerating performance of the drive, the motor is subjected to step speed commands of 500, 1000 and 1500 rpm at $t=0$, respectively. Fig. 4.2 shows the corresponding speed responses. From Fig. 4.2, one can see that the

transient responses are almost the same. It is indicated that the maximum available accelerating torque is always applied to speed up the speed response during transient operational mode.

Next, as an illustration of the rejection capability to lumped uncertainty, the motor is started from rest at $t=0$ up to 2100 rpm and T_L=0 Nm. The T_L is changed to $T_L = 0.3$ Nm at t=0.5 sec. Fig. 4.3 shows the corresponding trajectories of ω_r, i_{qs}, i_{ds}, s, i_{qf}^*, T_L and the expanded figure of ω_r for $t \in [0.49, 0.53]$. From Fig. 4.3, one can see some results as follows: i_{ds} will be changed automatically so that the minimum copper loss is achieved, s decay rapidly to zero, i_{qf}^* will reasonably reflect the change of T_L. Due to the fast reflection of i_{qf}^*, the fast recovery response can also be observed from Fig. 4.3.

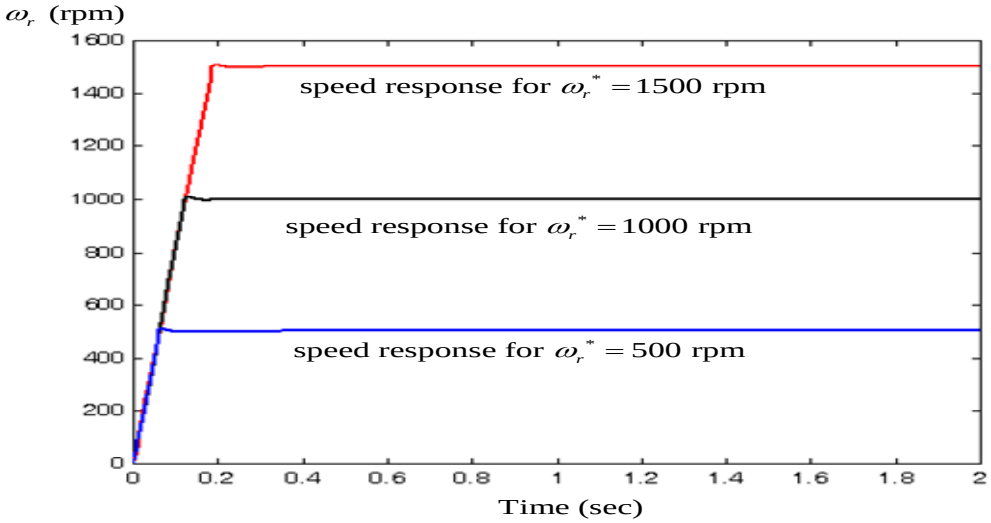

Fig. 4.2. Simulated trajectories of ω_r for step speed commands of 500, 1000, 1500 rpm, respectively.

Third, as a simulation for illustrating the high dynamics of the proposed adaptive sliding-mode speed controller, the motor is started from rest up to 2100 rpm and with $T_L = 0.3$ Nm. Fig. 4.4 shows the corresponding simulated traces of ω_r, i_{ds}, i_{qs} and $I_{qs\max}$. From Fig. 4.4, one can see that i_{qs} almost equal to $I_{qs\max}$ for $t \in [0, 0.55]$. It is indicated that the maximum accelerating torque is utilized to speed up the response.

Fourth, to show the rejection performance for an abrupt loading and unloading, the motor is started from rest up to 2200 rpm with $T_L = 0$ Nm and a pulse (0.3 Nm) external load torque T_L is applied for $t \in [0.5, 0.8]$. Fig. 4.5 shows the corresponding trajectories of ω_r, i_{ds} and the expanded figure of ω_r for $t \in [0.49, 0.9]$. From Fig. 4.5, a fast recovery response can be observed.

Fifth, to show the operation of the drive whose command is outside its operating range, the motor is subjected to a step speed command $\omega_r^* = 2400$ rpm and $T_L = 0.3$Nm. Fig. 4.6 shows the corresponding traces of ω_r, i_{ds}, i_{qs} and $I_{qs\max}$. From Fig. 4.6, one can see that $i_{qs} = I_{qs\max}$ for all time, which implies that the maximum torque is utilized to reduce the speed error. Although ω_r could not reach up to 2400 rpm, the operation of the drive is still stable.

Sixth, to show the operation of the automatic field weakening control, the motor is subjected to a step speed command 1200 rpm at t=0 and then set up to 2400 rpm at t=0.5 sec. Fig. 4.7 shows the corresponding trajectories of ω_r, i_{qs}, i_{ds} and s. From Fig. 4.7, one can see that i_{ds} will become negative automatically when the operation range enters into field weakening range. No region detector is required, the smooth transition can be observed clearly from the results.

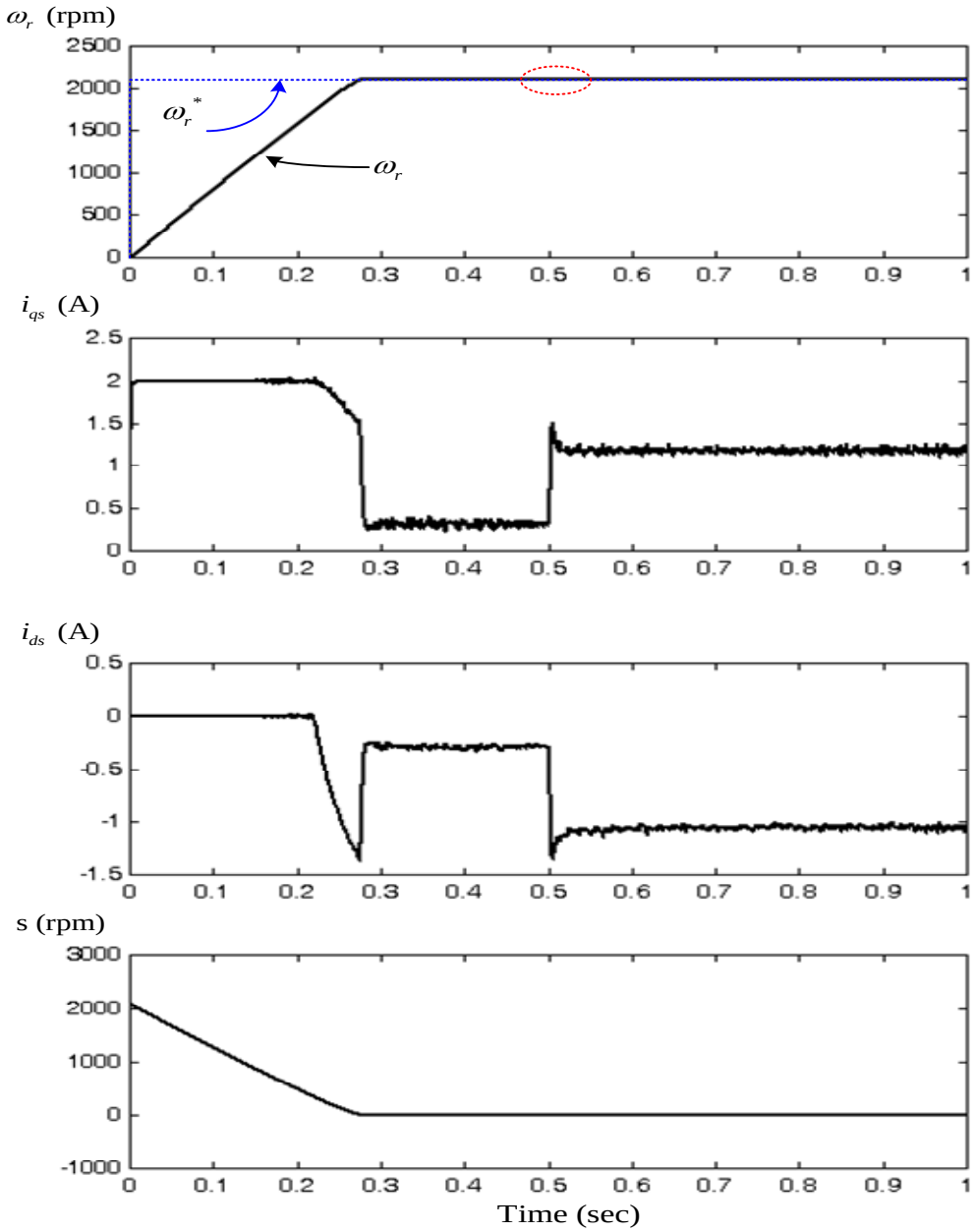

Fig. 4.3. Simulated trajectories of ω_r, i_{qs}, i_{ds}, s, i_{qf}^*, T_L and the expanded figure of ω_r for $t \in [0.49, 0.53]$, due to $\omega_r^* = 2100$ rpm and $T_L = 0.3$ Nm is applied at t=0.5 sec.

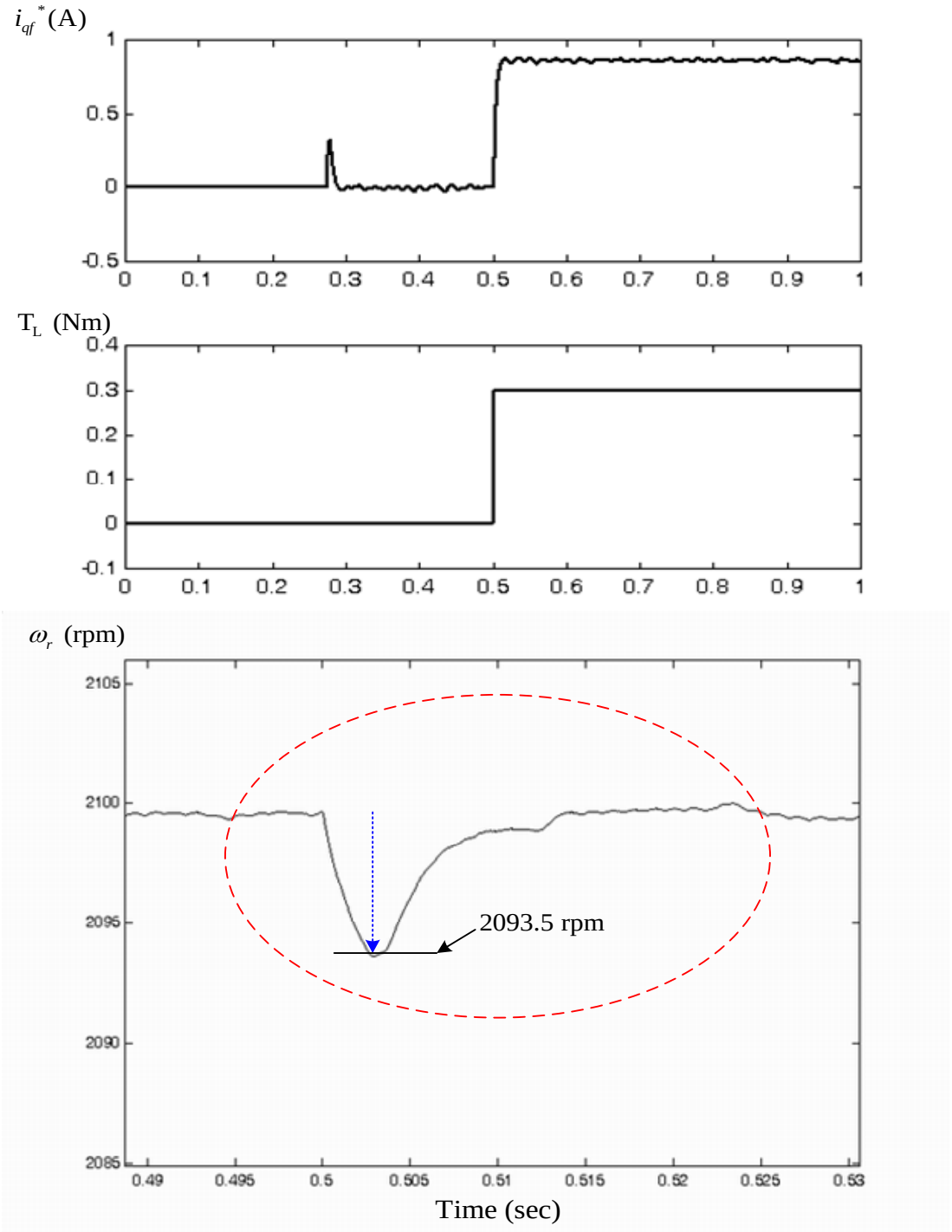

Fig. 4.3. Simulated trajectories of ω_r, i_{qs}, i_{ds}, s, i_{qf}^{*}, T_L and the expanded figure of ω_r for $t \in [0.49, 0.53]$, due to $\omega_r^* = 2100$ rpm and $T_L = 0.3$ Nm is applied at t=0.5 sec. (continued).

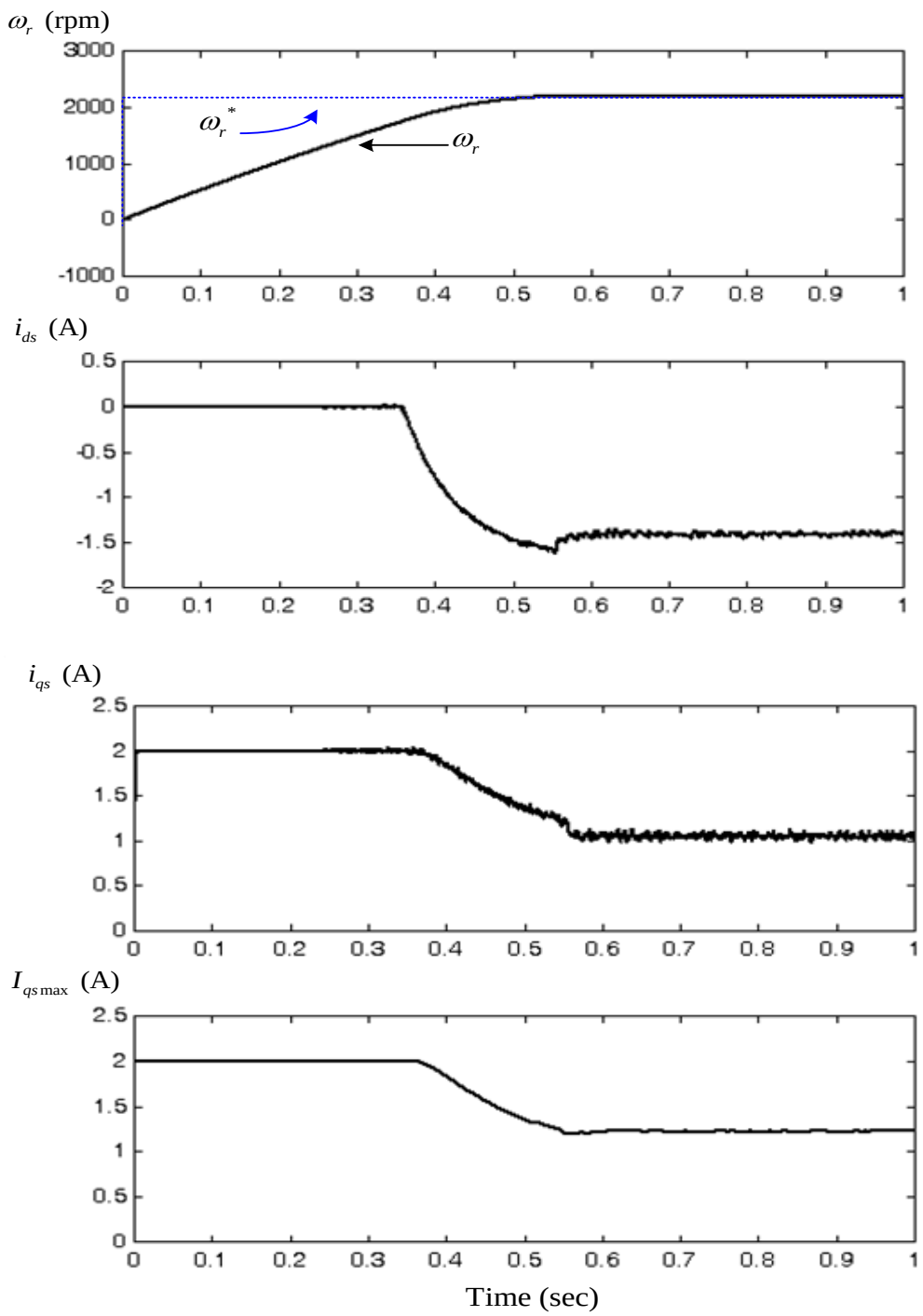

Fig.4.4. Simulated trajectories of ω_r , i_{ds} , i_{qs} and $I_{qs\max}$, due to $\omega_r^* = 2100$ rpm and $T_L = 0.3$ Nm .

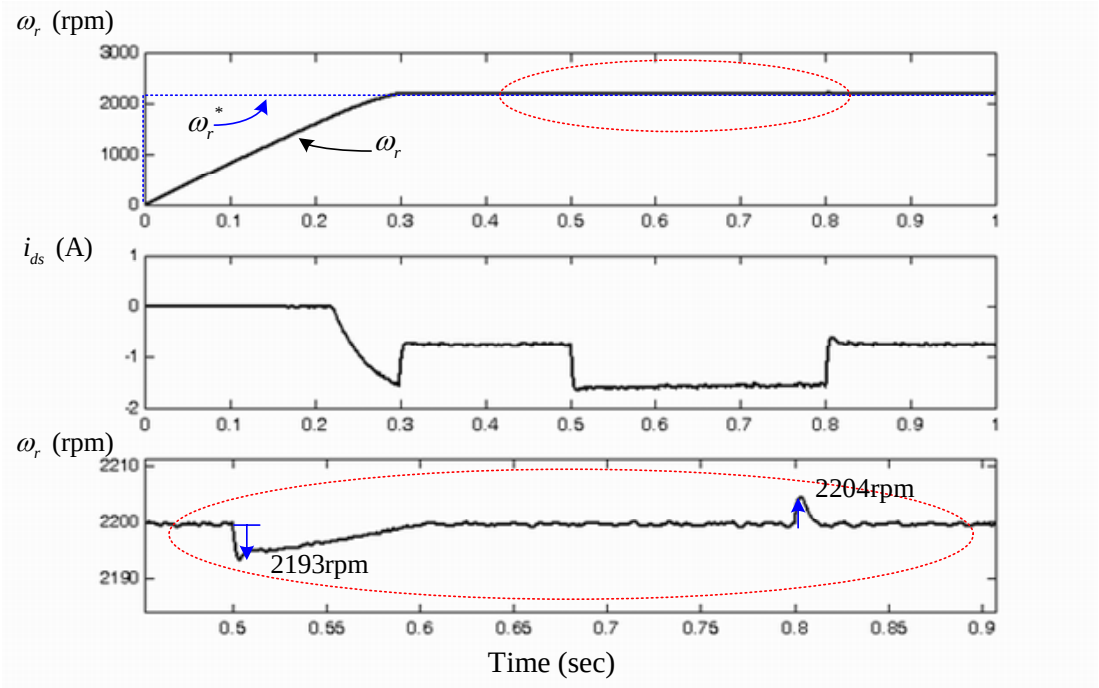

Fig. 4.5. Simulated trajectories of ω_r, i_{ds} and the expanded figure of ω_r for $t \in [0.49, 0.9]$, due to $\omega_r^* = 2100$ rpm and a pulse $T_L = 0.3$ Nm is applied.

Finally, to demonstrate that high dynamics performance can be achieved in spite of the variations of B and J, the motor is subjected to a step speed command of 2100 rpm. The same simulation is performed twice, one is with the parameters of $J = J_0$ and $B = B_0$ and the other is with the parameters of $J = 3J_0$ and $B = 3B_0$. Fig. 4.8 shows the corresponding trajectories of ω_r, i_{qs} and $I_{qs\max}$. From Fig. 4.8, one can see that i_{qs} almost equals to $I_{qs\max}$ for transient operation. It is indicated that the maximum torque is utilized for transient operation in spite of the triple variations of B and J.

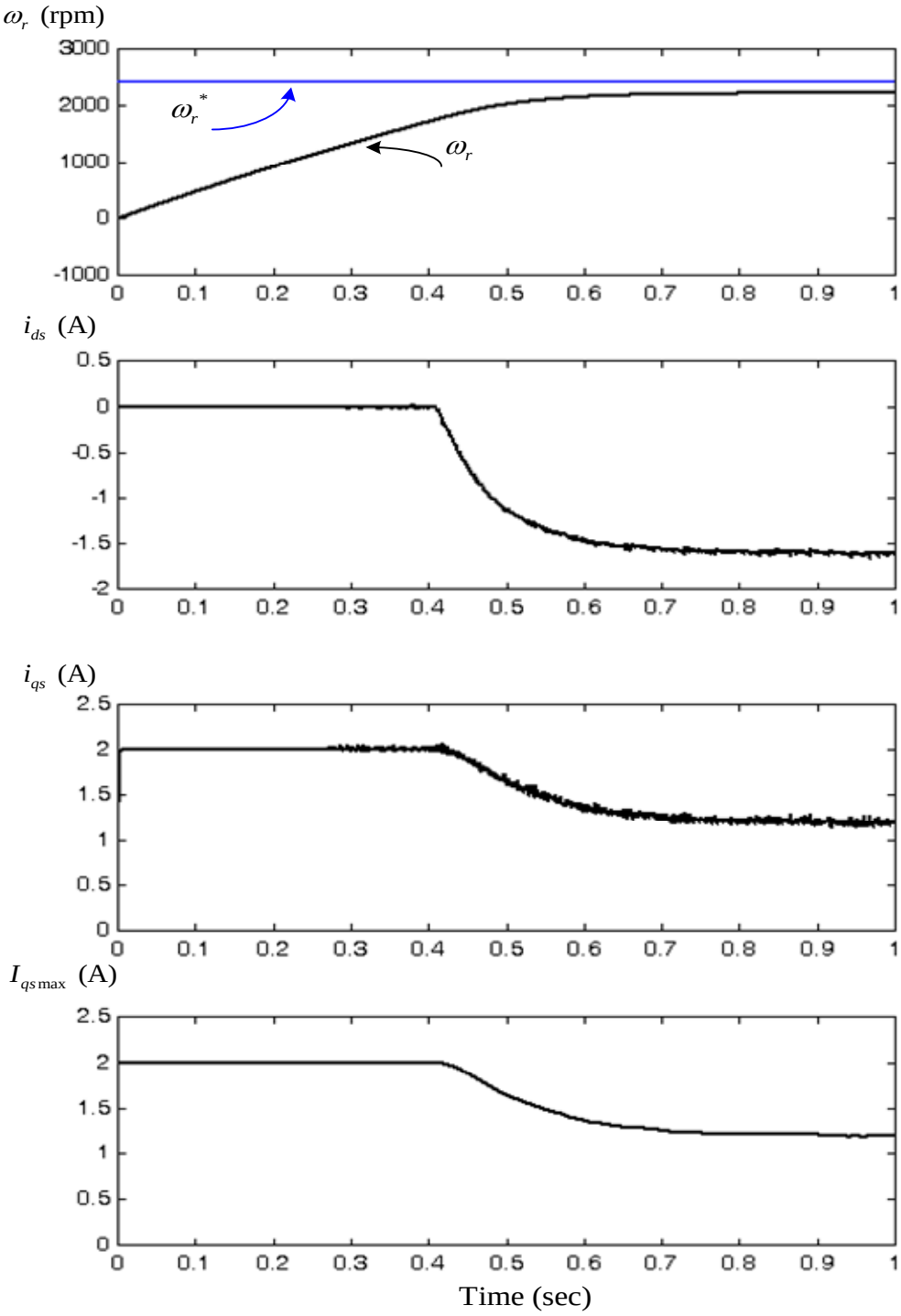

Fig. 4.6. Simulated trajectories of ω_r, i_{ds}, i_{qs} and $I_{qs\max}$ for step command $\omega_r^* = 2400\text{rpm}$ and $T_L = 0.3$ Nm.

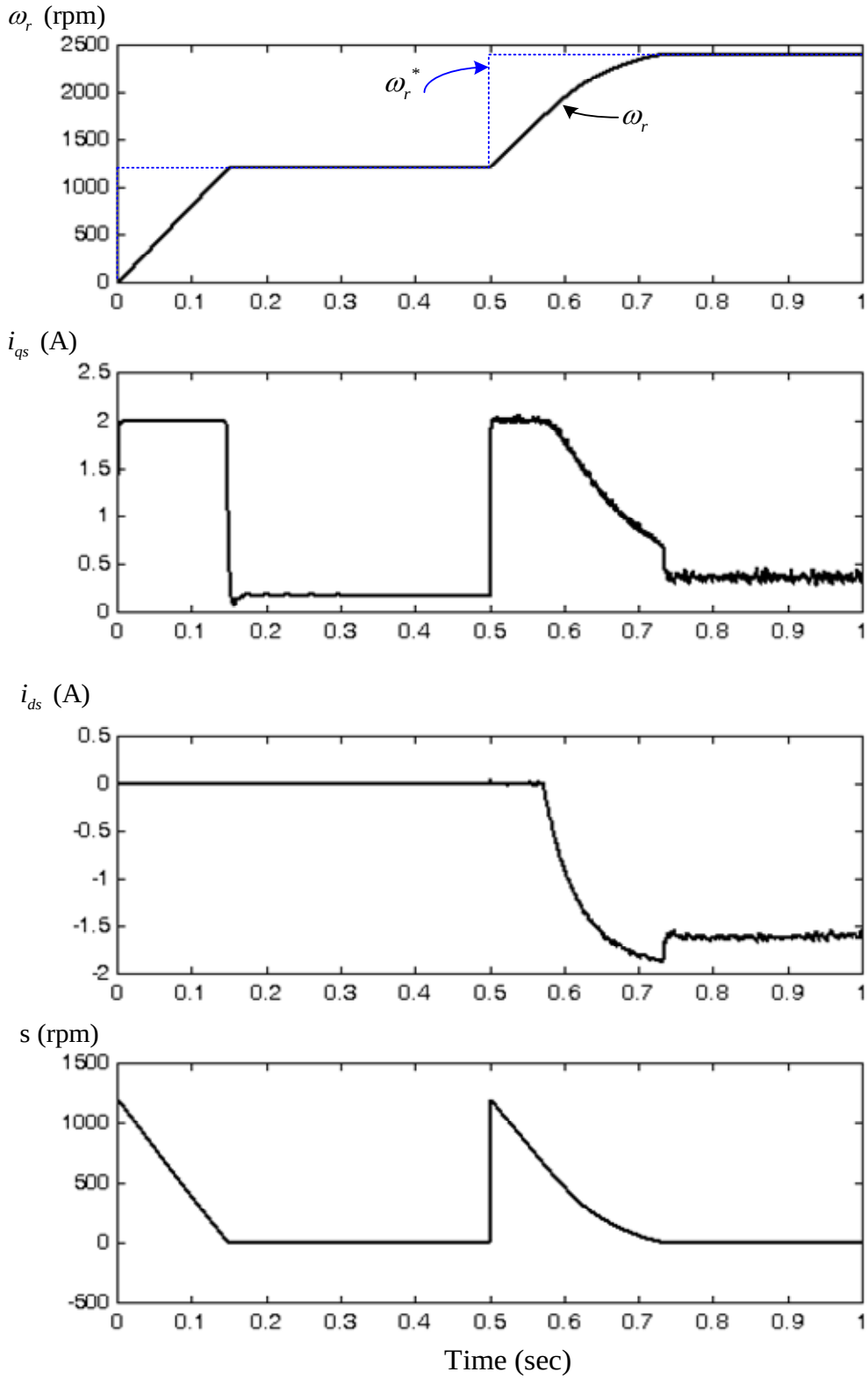

Fig. 4.7. Simulated trajectories of ω_r, i_{qs}, i_{ds} and s, due to step $\omega_r^* = 1200$rpm at t=0,0.5 sec.

As observed from above simulation results, one can see that the distinguishing features can be achieved by the proposed control strategy.

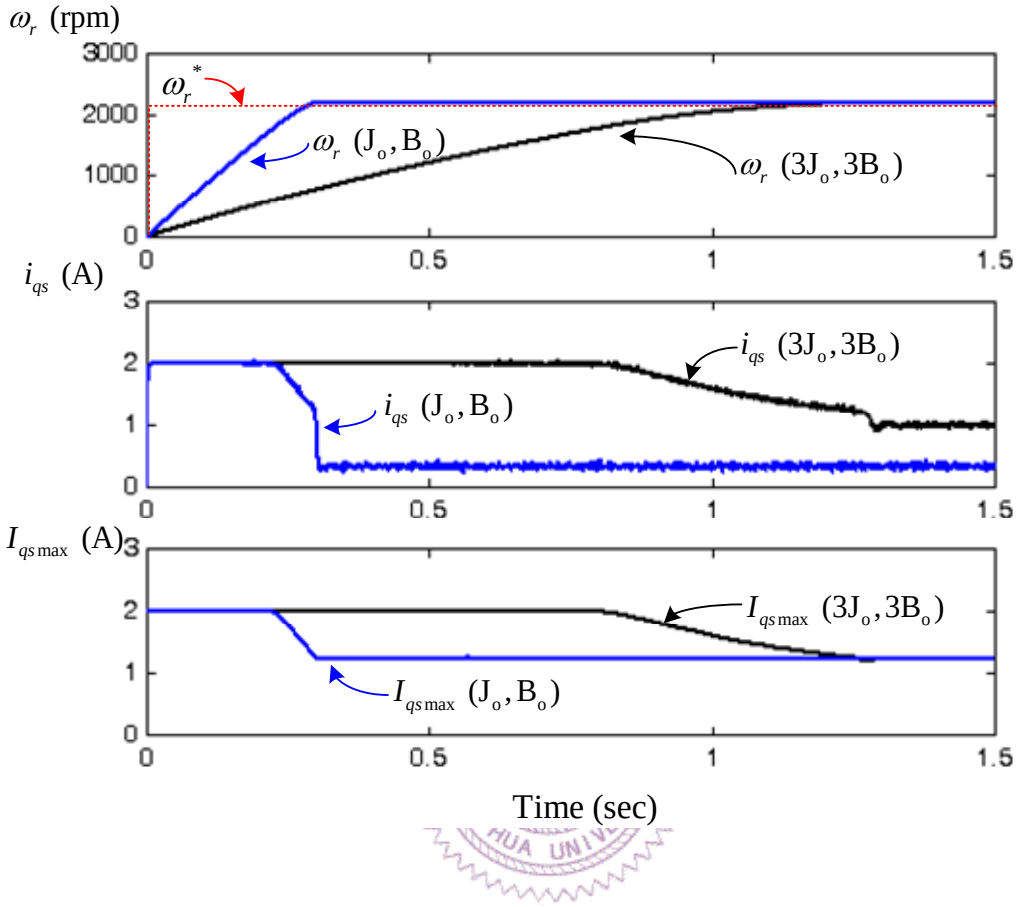

Fig. 4.8. Simulated trajectories of ω_r, i_{qs} and $I_{qs\max}$, for both (J_0, B_0) and $(3J_0, 3B_0)$.

4.4 Experimental Results

Several experimental results are provided below to show the performance of the proposed SMC speed controller. The implementation setup is the same as that depicted in the section 3.4 except the conventional PI speed controller is replaced by the proposed SMC speed controller.

First, to demonstrate the performance of the proposed SMC speed controller when the drive is operated on the constant torque limit region (region 1), the motor is started

from rest at t_0 up to 1200 rpm with $T_L = 0$ Nm and a pulse (0.3 Nm) external load torque T_L is applied for $t \in [t_1, t_2]$. Fig. 4.9 shows the corresponding trajectories of ω_r^*, ω_r, $\hat{f}$, i_{ds} and i_{qs}. From Fig. 4.9, one can see that the estimated lumped uncertainty, $\hat{f}$, can indeed track the variation of T_L. For clear demonstration of speed response, the expanded trajectories of that shown in Fig. 4.9 are shown in Fig. 4.10. From Fig. 4.10, one can see that almost no overshoot phenomenon and good rejection capability to the applied T_L can be observed from the expanded speed response.

Next, as an illustration of the rejection capability to external applied load torque when the drive is operated on field weakening region, the motor is started from rest at t_0 up to 2100 rpm with $T_L = 0$ Nm. A pulse external load torque (0.275 Nm) is applied for $t \in [t_1, t_2]$ and $t \in [t_3, t_4]$. Fig. 4.11 shows the corresponding trajectories of ω_r^*, ω_r, $\hat{f}$, i_{ds} and i_{qs}. As observed from Fig. 4.11, one can see that $\hat{f}$ can track the variation of T_L and i_{ds} can be changed to achieve minimum copper loss. For clear demonstration of the speed response, Fig. 4.12 shows the expanded figure of Fig. 4.11. Almost no overshoot and good rejection performance to the applied external load torque also can be achieved in spite the drive with SMC speed controller is operated in the field weakening region, as observed from the speed response shown in Fig. 4.11.

Third, to show the automatic field weakening control, the motor is subjected a step speed command 1200 rpm at $t = t_0$ and then step up to 2400 rpm at $t = t_0 + 1$ sec. Fig. 4.13 shows the corresponding trajectories of ω_r^*, ω_r, $\hat{f}$, i_{ds} and i_{qs}. From Fig. 4.13, one can see that i_{ds} will start to decrease when the motor speed approximately exceed 1737 rpm. It is indicated the drive enter to field weakening region (region 2).

Due to the mismatch of J and J_0, the estimated $\hat{f}$ would not kept being zero during the acceleration operation. However, the automatic field weakening control and the smooth transfer between different operation mode, namely zero d-axis current and field weakening control mode can be observed from Fig. 4.13.

Finally, as an experiment for illustrating the fast dynamics of the proposed adaptive sliding-mode speed controller for two-quadrant operation, Fig. 4.14 shows the responses of ω_r^*, ω_r, $\hat{f}$, i_{ds} and i_{qs} for a regular step change of speed command from 1200 rpm to 2400 rpm and then back to 1200 rpm. The 1200 rpm and 2400 rpm commands are fixed for 1.5 sec and 3 sec respectively. As the description in section 2.4, the smooth transient between the different operating modes and automatic filed weakening control effect can all be observed from Fig. 4.14. The fast speed response also can be observed from the acceleration and deceleration operation.

In summary, from the above simulation and experimental results, one can see that the following distinguishing features can be achieved by the proposed control strategy.

1). A good rejection performance to lumped uncertainty can be obtained.

2). Fast dynamic speed response can still be obtained in spite of the variations of B and J.

3). An adaptive sliding-mode speed controller with low chattering characteristic can be obtained through the adaptation strategy for the lumped uncertainty.

4).The automatic field weakening control and minimum copper loss are still achieved even when the conventional PI speed controller is replaced by the proposed adaptive sliding-mode speed controller.

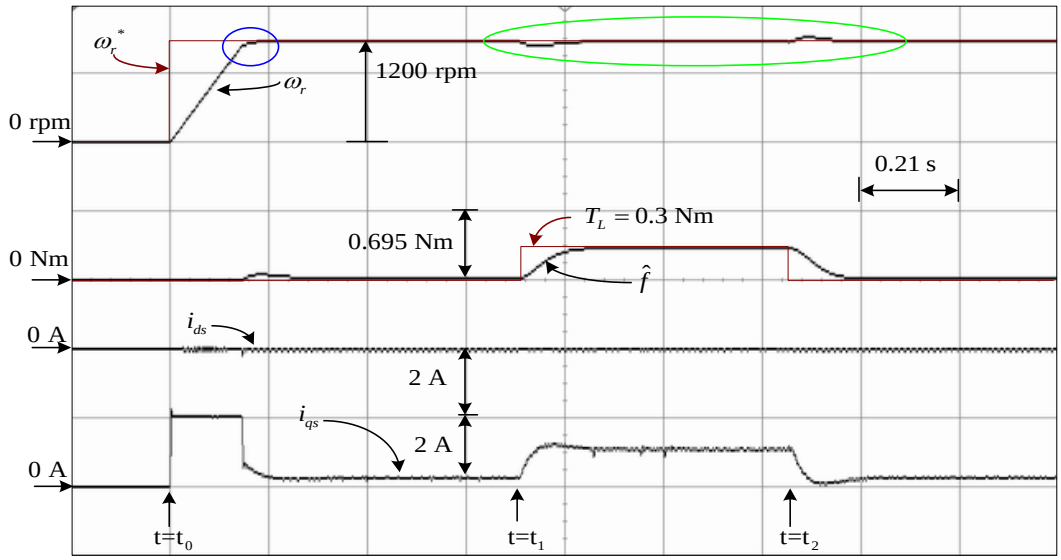

Fig. 4.9. Trajectories of ω_r^*, ω_r, $\hat{f}$, i_{ds} and i_{qs}, due to 1200 rpm step speed command and 0.3 Nm pulse load torque applied.

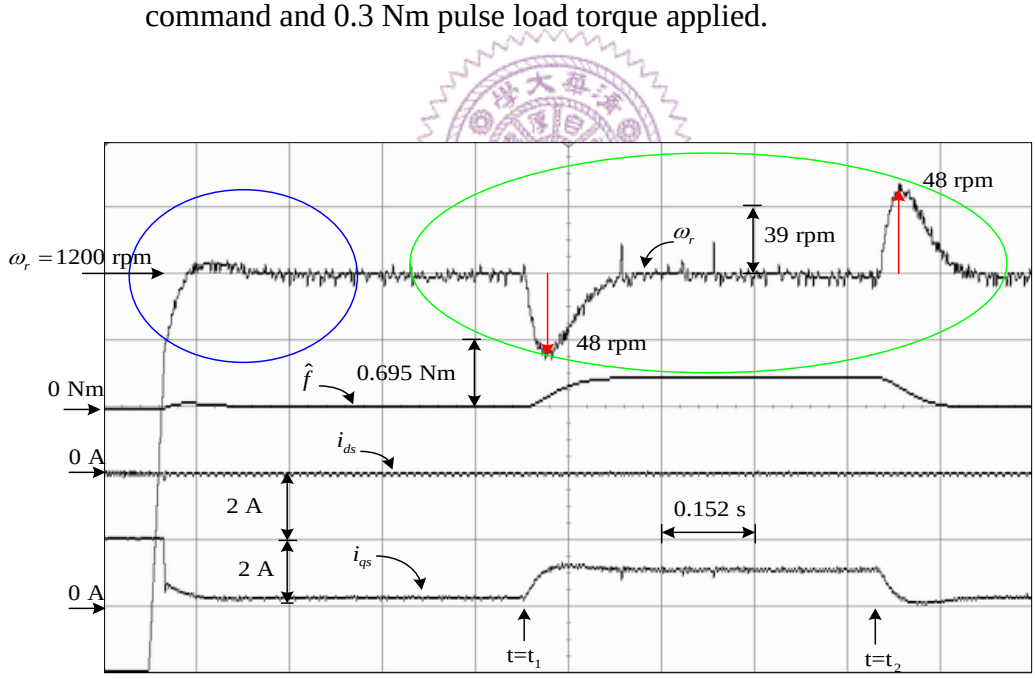

Fig. 4.10. Expanded trajectories of ω_r^*, ω_r, $\hat{f}$, i_{ds} and i_{qs}, due to 1200 rpm step speed command and 0.3 Nm pulse load torque applied.

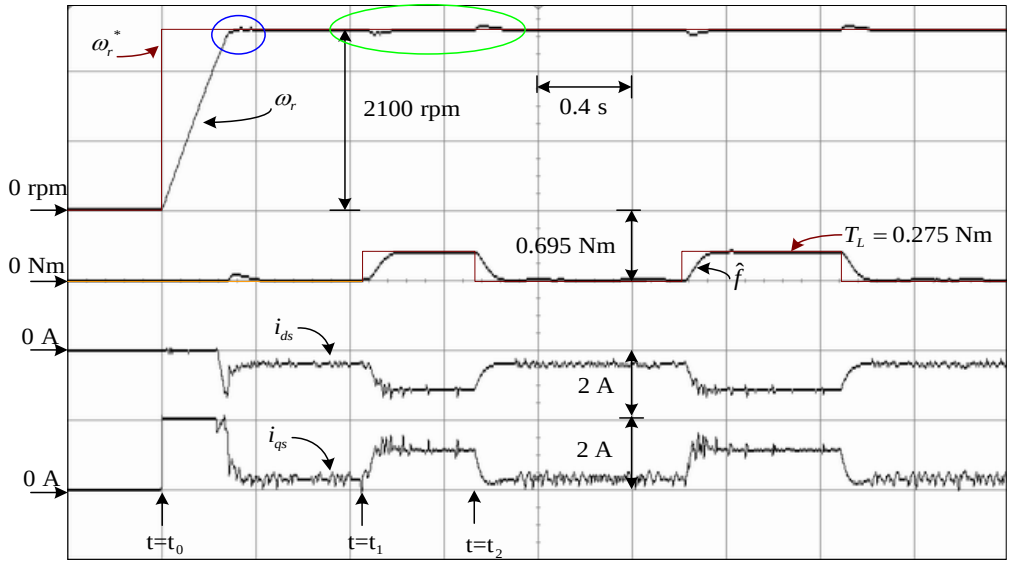

Fig. 4.11. Trajectories of ω_r^*, ω_r, $\hat{f}$, i_{ds} and i_{qs}, due to 2100 rpm step speed command and 0.275 Nm pulse load torque applied.

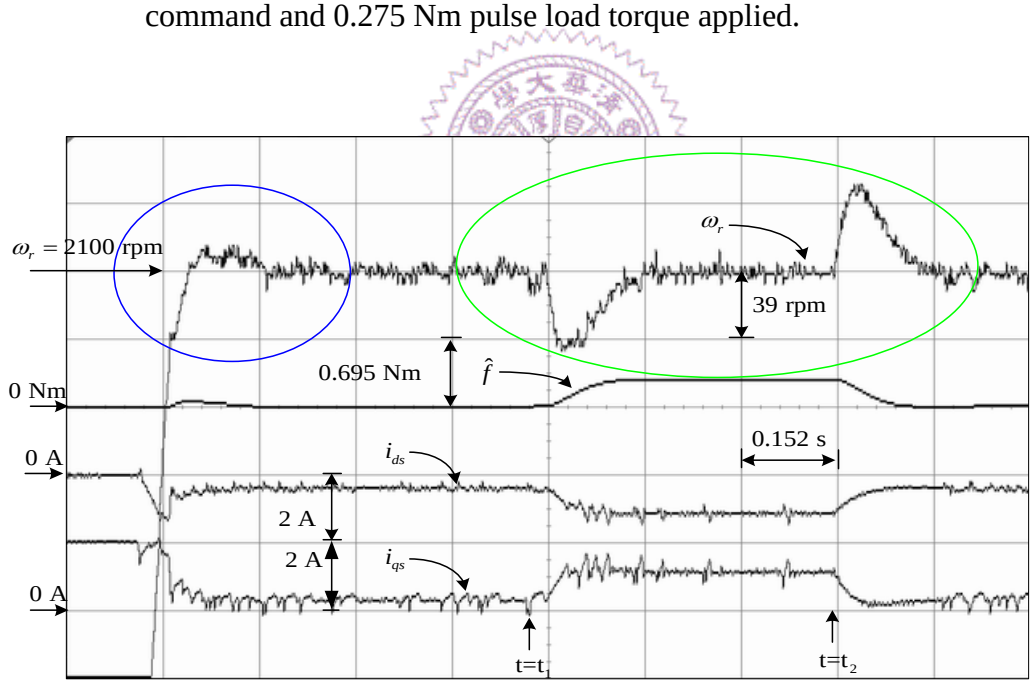

Fig. 4.12. Expanded trajectories of ω_r^*, ω_r, $\hat{f}$, i_{ds} and i_{qs}, due to 2100 rpm step speed command and 0.275 Nm pulse load torque applied.

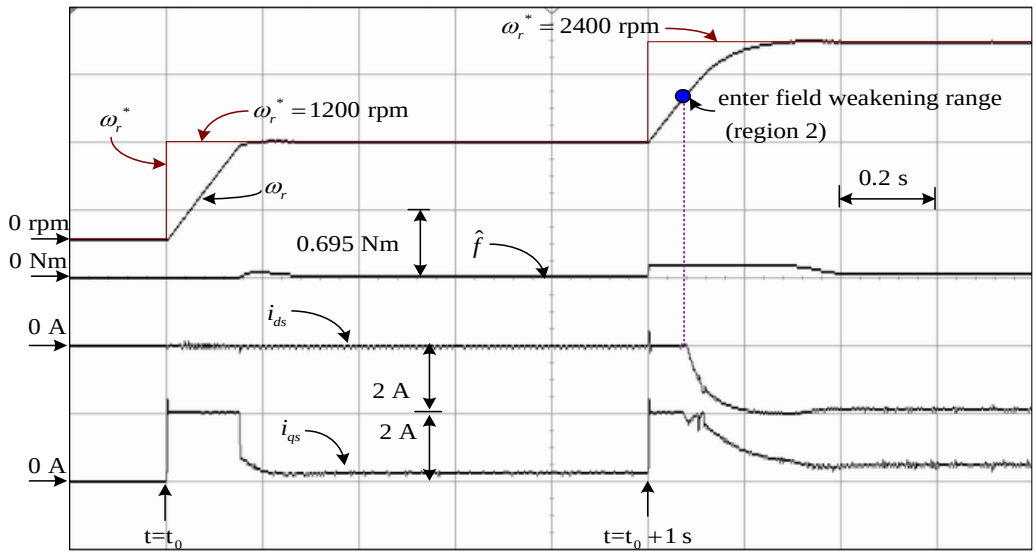

Fig. 4.13. Trajectories of ω_r^*, ω_r, $\hat{f}$, i_{ds} and i_{qs}, due to $\omega_r^* = 1200$ rpm at $t = t_0, t_0 + 1$ sec.

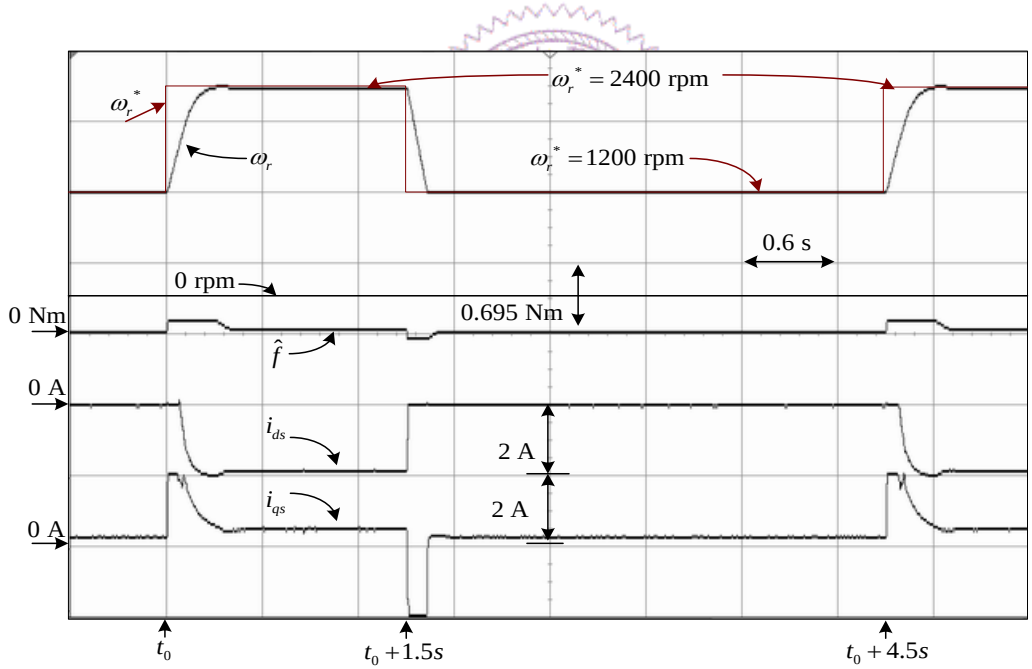

Fig. 4.14. Trajectories of ω_r^*, ω_r, $\hat{f}$, i_{ds} and i_{qs} for the proposed control strategy operated in two quadrant operation.